Hindawi
Mathematical Problems in Engineering
Volume 2023, Article ID 8897781, 9 pages
https://doi.org/10.1155/2023/8897781

Research Article

Active RIS-Assisted Transmission Design for Wireless Secrecy Network with Energy Harvesting

Ping Li and Jinhong Bian

School of Information Technology, Yancheng Institute of Technology, Yancheng 224051, China

Correspondence should be addressed to Ping Li; infoliping@ycit.edu.cn and Jinhong Bian; bianjh@ycit.edu.cn

Received 10 December 2022; Revised 2 January 2023; Accepted 17 January 2023; Published 1 February 2023

Academic Editor: Jie Hu

We investigated the secrecy transmission design in a simultaneous wireless information and power transfer (SWIPT) system, where an active reconfigurable intelligent surface (RIS) is utilized to enhance the secure information transmission as well as the wireless energy transmission. Specifically, we studied the fairness secrecy rate maximization by jointly optimizing the transmit beamformer and the reflecting coefficients, subject to the transmit power constraint and the nonlinear energy harvesting constraint. To solve the formulated nonconvex problem, we utilize the successive convex approximation to reformulate the problem and then propose an alternating optimization to address the approximated problem. The simulation result showed the performance of the proposed design as well as the superiority of active RIS when compared with other benchmarks.

1. Introduction

Future wireless networks will meet an increasing requirement for wireless applications such as high spectral efficiency and low power consumption [1]. Since battery capacity is limited, the dual use of radio frequency (RF) signals for enabling simultaneous wireless information and power transfer (SWIPT) has attracted intense interest [2].

On the other hand, due to the broadcast character of the wireless channel, the signal sent to the legitimate user maybe eavesdropped by the eavesdropper (Eve) [3]. Normally, to achieve SWIPT efficiently, the energy receiver (ER) is deployed closer to the transmitter (Tx) than the information receiver (IR) to help energy harvesting (EH). However, when the ER tries to decode the confidential information sent to the IR, it will pose a great threat to communication security [4]. To address this issue, physical layer security (PLS) techniques have been proposed to improve the secrecy performance in wireless networks, which utilizes the randomness of the wireless channel to achieve secure communication at the physical layer [5].

Nowadays, reconfigurable intelligent surface (RIS) has emerged as a promising technique for the wireless network. The RIS is a planar array with several low-cost reflecting elements, which can alter the incident signal passively [6]. Since it only reflects the received signal, the hardware and power cost for RIS are much lower than the traditional active transmitter or relay [7]. With these advantages, the RIS has sparked great research interests, such as the nonorthogonal multiple access (NOMA) networks [8], the SWIPT networks [9], the hybrid satellite-terrestrial networks [10], the multicell network [11], and the mobile edge computing (MEC) network in [12], where a passive RIS and relay-assisted MEC scheme was proposed.

Meanwhile, since RIS can enhance or weak the signal power in different directions, thus it is beneficial to secure transmission design and optimization. To be specific, the authors of [13] investigated the secrecy rate maximization in a downlink multiple-input single-output (MISO) network assisted by a RIS. Then, the authors of [14] studied the secure transmission with multilayer RIS architecture. The authors of [15] studied the energy-efficient beamformer and cooperative jamming design for RIS-assisted networks. Also, the authors of [16] studied the RIS-enhanced secure scheme against both eavesdropping and jamming.

However, the reflecting signals suffer from large-scale fading twice. To mitigate this "double fading" effect, a new concept called active RIS has been proposed in [17], where each unit is equipped with active amplification [18]. Then, the authors of [19] studied the optimization technique for active RIS. The authors of [20] compared whether active RIS is superior to passive RIS. Recently, the authors of [21] studied the active RIS-aided secure transmission, where a semidefinite relaxation (SDR) method was proposed to maximize the secrecy rate. Then, the authors of [22, 23] investigated the active RIS-assisted secure transmission for satellite terrestrial networks, and the results suggested the superiority of active RIS when compared with passive RIS in improving the secrecy rate and secrecy energy efficiency performances, respectively.

Motivated by this, this work investigates the effect of an active RIS in the SWIPT network. Specifically, by considering individual IRs and ERs, as well as the nonlinear EH model, we handle the fairness secrecy rate maximization objective by jointly designing the transmit beamformer (BF) and the reflecting coefficient (RC), subject to the EH constraints. We utilize the successive convex approximation (SCA) method to recast the problem, and then, an alternating optimization (AO) algorithm is proposed. Besides, the computational complexity is analyzed. The simulation result showed the performance of the proposed design. Our main contribution is as follows:

(1) We propose to use active RIS to improve the secure performance of the SWIPT network, as well as to alleviate the "double fading." Specifically, we aim to maximize the minimal secrecy rate of the IRs by jointly optimizing the transmit BF and the RC, subject to the nonlinear EH constraints and the transmit power constraints.

(2) The formulated problem is nonconvex due to the nonsmooth max-min secrecy rate objective and the nonconvex EH constraint. To handle this obstacle, we recast the original problem into a quasi-convex problem. Then, we propose an AO algorithm, which optimizes the variables alternatingly. Besides, the proposed algorithm enjoys polynomial-time computational complexity, which is beneficial to implement.

(3) Simulation results show the performance gains of the proposed designs as well as the superiority of active RIS, which not only effectively relieve the "double fading" effect but also enhance the secure performance when compared with other baselines.

Although some works such as [2–4, 21] have studied the PLS issue or the energy harvesting issue, however, the differences between our work with these works can be summarized as follows: (1) the system model of our work is quite different with these works. Only the authors of [21] studied the active RIS-assisted secure transmission while the others are related to relay. In addition, the authors of [3, 21] are not related to SWIPT while the authors of [2, 4] are not focus on security communication; (2) the formulated problem and optimization method of our work are quite different with these works. We propose an AO with an SCA-based algorithm to maximize the minimal secrecy rate among these users while guaranteeing the harvested power at each ER exceeds the given threshold. Such a problem has not been studied in these works.

The rest part is organized as follows. A system model description and problem formulation are given in Section 2. Section 3 develops an AO-based optimization approach. Simulation results are illustrated in Section 4. Finally, Section 5 finishes the paper.

Notations: The transpose, conjugate transpose, and trace of a matrix $\mathbf{A}$ are denoted as $\mathbf{A}^T$, $\mathbf{A}^H$, and $\mathrm{Tr}(\mathbf{A})$, respectively. $\|\mathbf{A}\|_F$ denotes the Frobenius norm of matrix $\mathbf{A}$. $\mathrm{Diag}(\mathbf{a})$ is a diagonal matrix with $\mathbf{a}$ on the main diagonal. $\Re\{a\}$ denotes the real part. $\mathcal{CN}(0, \mathbf{A})$ denotes a circularly symmetric complex Gaussian random vector with mean 0 and covariance $\mathbf{A}$.

2. System Model and Problem Formulation

2.1. System Model. As shown in Figure 1, the network consists of one Tx, one RIS, K IRs, and L ERs. The Tx has N antennas, and the RIS has M elements. In addition, each IR/ER is the single antenna. The channel between Tx and the k-th IR/l-th ER is denoted as $\mathbf{h}_{T,k} \in \mathbb{C}^{N\times 1}$ and $\mathbf{g}_{T,l} \in \mathbb{C}^{N\times 1}$. And the channel between Tx and the RIS is denoted as $\mathbf{F} \in \mathbb{C}^{M\times N}$, and the channel between the RIS and the k-th IR/l-th ER is denoted as $\mathbf{h}_{R,k} \in \mathbb{C}^{M\times 1}$ and $\mathbf{g}_{R,l} \in \mathbb{C}^{M\times 1}$.

Then, we introduce the mathematical model of active RIS. To be specific, the RC matrix of the active RIS is given by $\Phi = \mathrm{Diag}(\phi_1, \ldots, \phi_M) \in \mathbb{C}^{M\times M}$, where the RC of the m-th element is denoted as $\phi_m = \alpha_m e^{j\theta_m}$, with α_m and θ_m being the amplitude and the phase within the intervals $\alpha_m \in [0, \alpha_{m,\max}]$ and $\theta_m \in [0, 2\pi$. For active RIS, $\alpha_{m,\max}$ can be larger than 1.

Let $s_k \in \mathbb{C}$ denote the symbol for the k-th IR. The transmit signal $\mathbf{x}$ is

$$\mathbf{x} = \sum_{k=1}^{K} \mathbf{w}_k s_k + \mathbf{w}_0, \tag{1}$$

where $\mathbf{w}_k \in \mathbb{C}^{N\times 1}$ is the BF for the k-th IR, and $\mathbf{w}_0 \in \mathbb{C}^{N\times 1}$ is the AN to deteriorate the reception of the information at the ER.

Thus, the received signal at the k-th IR/ER is

$$y_{i,k} = \left(\mathbf{h}_{T,k}^H + \mathbf{h}_{R,k}^H \mathbf{\Phi F}\right)x + \mathbf{h}_{R,k}^H \mathbf{\Phi n}_r + n_{i,k}, \tag{2a}$$

$$y_{e,l} = \left(\mathbf{g}_{T,l}^H + \mathbf{g}_{R,l}^H \mathbf{\Phi F}\right)x + \mathbf{g}_{R,l}^H \mathbf{\Phi n}_r + n_{e,l}, \tag{2b}$$

where $n_{i,k}$ and $n_{e,l}$ denote the noise at the k-th IR and the l-th ER with $n_{i,k} \sim \mathcal{CN}(0, \sigma_{i,k}^2)$ and $n_{e,l} \sim \mathcal{CN}(0, \sigma_{e,l}^2)$. In addition, $\mathbf{n}_r$ is the noise at the RIS with $\mathbf{n}_r \sim \mathcal{CN}(0, \sigma_r^2)$.

Thus, the signal-to-interference-noise ratio (SINR) for the k-th IR is

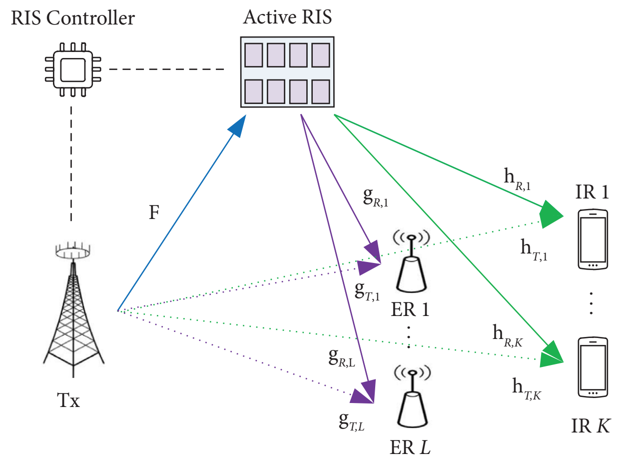

FIGURE 1: System model.

$$\Gamma_k = \frac{\left|\left(\mathbf{h}_{T,k}^H + \mathbf{h}_{R,k}^H \mathbf{\Phi}\mathbf{F}\right)\mathbf{w}_k\right|^2}{\sum_{j=0,j\neq k}^{K}\left|\left(\mathbf{h}_{T,k}^H + \mathbf{h}_{R,k}^H \mathbf{\Phi}\mathbf{F}\right)\mathbf{w}_j\right|^2 + \sigma_r^2\left\|\mathbf{h}_{R,k}^H\mathbf{\Phi}\right\|^2 + \sigma_{i,k}^2}. \quad (3)$$

When the l-th ER try to eavesdrop the confidential message send to the k-th IR, the SINR is given by

$$\Gamma_{k,l} = \frac{\left|\left(\mathbf{g}_{T,l}^H + \mathbf{g}_{R,l}^H \mathbf{\Phi}\mathbf{F}\right)\mathbf{w}_k\right|^2}{\sum_{j=0,j\neq k}^{K}\left|\left(\mathbf{g}_{T,l}^H + \mathbf{g}_{R,l}^H \mathbf{\Phi}\mathbf{F}\right)\mathbf{w}_j\right|^2 + \sigma_r^2\left\|\mathbf{g}_{R,l}^H\mathbf{\Phi}\right\|^2 + \sigma_{e,l}^2}. \quad (4)$$

Thus, the secrecy rate for the k-th IR is

$$R_k = \log_2\left(1+\Gamma_k\right) - \max_l \log_2\left(1+\Gamma_{k,l}\right). \quad (5)$$

And the harvested power at the antenna for the l-th ER is

$$E_l^{\text{in}} = \sum_{k=0}^{K}\left|\left(\mathbf{g}_{T,l}^H + \mathbf{g}_{R,l}^H \mathbf{\Phi}\mathbf{F}\right)\mathbf{w}_k\right|^2 + \sigma_r^2\left\|\mathbf{g}_{R,l}^H\mathbf{\Phi}\right\|^2. \quad (6)$$

Here, we employ a nonlinear EH model, which is given as

$$E_l^{\text{prac}} = \Psi^{\text{prac}}\left(E_l^{\text{in}}\right) \triangleq \frac{R_l/1 + e^{-a_l\left(E_l^{\text{in}} - b_l\right)} - \left(R_l/1 + e^{a_l b_l}\right)}{1 - \left(1/1 + e^{a_l b_l}\right)}, \quad (7)$$

where E_l^{prac} denotes the practical output power for the EH circuit, and R_l is a constant meaning the maximum harvested power when the EH circuit saturates. a_l and b_l are constants determined by the circuit. For more details about the nonlinear EH model, readers can refer to [24].

2.2. Problem Formulation. Our problem is to design $\mathbf{w}_k$ and Φ, such that the minimal secrecy rate among these IRs can be maximized while guaranteeing the harvested power at each ER is exceed the given threshold. Thus, the problem is

$$\max_{\mathbf{w}_k,\mathbf{\Phi}} G\left(\mathbf{w}_k,\mathbf{\Phi}\right) \triangleq \min_k R_k, \quad (8a)$$

$$\text{s.t. } E_l^{\text{prac}} \geq E_{th}, \quad (8b)$$

$$\sum_{k=0}^{K}\left\|\mathbf{\Phi}\mathbf{F}\mathbf{w}_k\right\|^2 + \sigma_r^2\left\|\mathbf{\Phi}\right\|^2 \leq P_r, \quad (8c)$$

$$\sum_{k=0}^{K}\left\|\mathbf{w}_k\right\|^2 \leq P_s, \quad (8d)$$

$$\alpha_m \leq \alpha_{m,\max}, \quad (8e)$$

where P_r and P_s stand for the total power constraint for the RIS and Tx.

3. The Proposed Method

Firstly, we turn (8b) to the following constraint $E_l^{\text{in}} \geq \Omega_l^{\text{in}}$, where

$$\Omega_l^{\text{in}} = b_l - \mathrm{In}\frac{\left(M_l/E_{\text{th}}\left(1-\left(1/1+e^{a_l b_l}\right)\right) + \left(M_l/1+e^{a_l b_l}\right) - 1\right)}{a_l}. \quad (9)$$

The detailed procedure is given in the Appendix. Thus, (8b) is recast as

$$\sum_{k=0}^{K}\left|\left(\mathbf{g}_{T,l}^H + \mathbf{g}_{R,l}^H \mathbf{\Phi}\mathbf{F}\right)\mathbf{w}_k\right|^2 + \sigma_r^2\left\|\mathbf{g}_{R,l}^H\mathbf{\Phi}\right\|^2 \geq \Omega_i^{\text{in}}. \quad (10)$$

3.1. The AO Procedure. Firstly, we handle the max–min information rate objective. In fact, by introducing the slack variable τ_k, r_k, and $\lambda_{k,l}$, $\forall k, \forall l$, (8a)–(8d) can be reformulated as

$$\max_{\mathbf{w}_k,\mathbf{\Phi},r_k,\tau_k,\lambda_{k,l}} \min \tau_k, \quad (11a)$$

$$\text{s.t. } \tau_k \leq \log_2\left(r_k\lambda_{k,l}\right), \forall k, \forall l, \quad (11b)$$

$$1 + \frac{\left|\left(\mathbf{h}_{T,k}^H + \mathbf{h}_{R,k}^H \mathbf{\Phi}\mathbf{F}\right)\mathbf{w}_k\right|^2}{\sum_{j=0,j\neq k}^{K}\left|\left(\mathbf{h}_{T,k}^H + \mathbf{h}_{R,k}^H \mathbf{\Phi}\mathbf{F}\right)\mathbf{w}_j\right|^2 + \sigma_r^2\left\|\mathbf{h}_{R,k}^H\mathbf{\Phi}\right\|^2 + \sigma_{i,k}^2} \geq r_k, \quad (11c)$$

$$1 + \frac{\left|\left(\mathbf{g}_{T,k}^H + \mathbf{g}_{R,k}^H \mathbf{\Phi}\mathbf{F}\right)\mathbf{w}_k\right|^2}{\sum_{j=0,j\neq k}^{K}\left|\left(\mathbf{g}_{T,k}^H + \mathbf{g}_{R,k}^H \mathbf{\Phi}\mathbf{F}\right)\mathbf{w}_j\right|^2 + \sigma_r^2\left\|\mathbf{g}_{R,k}^H\mathbf{\Phi}\right\|^2 + \sigma_{e,l}^2} \leq \frac{1}{\lambda_{k,l}}, \quad (11d)$$

$$(8c), (8d), (8e) \quad (11e)$$

(11b) is equivalent to $2^{\tau_k+2} + (r_k - \lambda_{k,l})^2 \leq (r_k + \lambda_{k,l})^2$, which can be further recast as a second-order cone constraint as $\|[\sqrt{2^{\tau_k+2}}, r_k - \lambda_{k,l}]\| \leq r_k + \lambda_{k,l}$.

Then, (11c) can be reformulated as

$$\frac{\left|\left(\mathbf{h}_{T,k}^H + \mathbf{h}_{R,k}^H \mathbf{\Phi}\mathbf{F}\right)\mathbf{w}_k\right|^2}{r_k - 1} \geq \sum_{j=0,j\neq k}^{K}\left|\left(\mathbf{h}_{T,k}^H + \mathbf{h}_{R,k}^H \mathbf{\Phi}\mathbf{F}\right)\mathbf{w}_j\right|^2 + \sigma_r^2\left\|\mathbf{h}_{R,k}^H\mathbf{\Phi}\right\|^2 + \sigma_{i,k}^2. \quad (12)$$

Besides, (11d) can be equivalently rewritten as

$$\frac{\sum_{j=0,j\neq k}^{K}\left|\left(\mathbf{g}_{T,k}^{H}+\mathbf{g}_{R,k}^{H}\mathbf{\Phi}\mathbf{F}\right)\mathbf{w}_{j}\right|^{2}+\sigma_{r}^{2}\left\|\mathbf{g}_{R,k}^{H}\mathbf{\Phi}\right\|^{2}+\sigma_{e,l}^{2}}{\lambda_{k,l}} \geq \sum_{k=0}^{K}\left|\left(\mathbf{g}_{T,k}^{H}+\mathbf{g}_{R,k}^{H}\mathbf{\Phi}\mathbf{F}\right)\mathbf{w}_{j}\right|^{2}+\sigma_{r}^{2}\left\|\mathbf{g}_{R,k}^{H}\mathbf{\Phi}\right\|^{2}+\sigma_{e,l}^{2}. \tag{13}$$

However, (12) and (13) are all nonconvex, since the difference between the two quadratic forms is neither convex nor concave. To handle the above obstacles, we follow the constrained convex procedure by replacing these functions with first-order expansions. Specifically, we denote $f_{Y,y}(\mathbf{v},v)=\mathbf{v}^{H}\mathbf{Y}\mathbf{v}/v-y$ for $\mathbf{Y}\succcurlyeq 0$ and $v\geq y$, at a certain point $(\tilde{\mathbf{v}},\tilde{v})$, and the first-order Taylor expansion of the function is $F_{\mathbf{Y},y}(\mathbf{v},v,\tilde{\mathbf{v}},\tilde{v})=2\Re\{\tilde{\mathbf{v}}^{H}\mathbf{Y}\mathbf{v}\}/\tilde{v}-y-\tilde{\mathbf{v}}^{H}\mathbf{Y}\tilde{\mathbf{v}}/(\tilde{v}-y)^{2}(v-y)$ [25].

By adopting the above Taylor expansion, when fixing Φ, at the given points $(\tilde{\mathbf{w}}_k,\tilde{r}_k,\tilde{\lambda}_{l,k})$, (12) can be transformed as

$$\frac{2\Re\left\{\tilde{\mathbf{w}}_{k}^{H}\left(\mathbf{h}_{T,k}^{H}+\mathbf{h}_{R,k}^{H}\mathbf{\Phi}\mathbf{F}\right)^{H}\left(\mathbf{h}_{T,k}^{H}+\mathbf{h}_{R,k}^{H}\mathbf{\Phi}\mathbf{F}\right)\mathbf{w}_{k}\right\}}{\tilde{r}_{k}-1}-\frac{\left|\left(\mathbf{h}_{T,k}^{H}+\mathbf{h}_{R,k}^{H}\mathbf{\Phi}\mathbf{F}\right)\tilde{\mathbf{w}}_{k}\right|^{2}}{\left(\tilde{r}_{k}-1\right)^{2}}\left(r_{k}-1\right) \geq \sum_{j=0,j\neq k}^{K}\left|\left(\mathbf{h}_{T,k}^{H}+\mathbf{h}_{R,k}^{H}\mathbf{\Phi}\mathbf{F}\right)\mathbf{w}_{j}\right|^{2}+\sigma_{r}^{2}\left\|\mathbf{h}_{R,k}^{H}\mathbf{\Phi}\right\|^{2}+\sigma_{i,k}^{2}. \tag{14}$$

Similarly, (13) can be approximated as

$$\frac{\sum_{j=0,j\neq k}^{K}2\Re\left\{\tilde{\mathbf{w}}_{j}^{H}\left(\mathbf{g}_{T,k}^{H}+\mathbf{g}_{R,k}^{H}\mathbf{\Phi}\mathbf{F}\right)^{H}\left(\mathbf{g}_{T,k}^{H}+\mathbf{g}_{R,k}^{H}\mathbf{\Phi}\mathbf{F}\right)\mathbf{w}_{j}\right\}}{\tilde{\lambda}_{k,l}}-\frac{\sum_{j=0,j\neq k}^{K}\left|\left(\mathbf{g}_{T,k}^{H}+\mathbf{g}_{R,k}^{H}\mathbf{\Phi}\mathbf{F}\right)\tilde{\mathbf{w}}_{j}\right|^{2}}{\tilde{\lambda}_{k,l}^{2}}\lambda_{k,l}+\left(\sigma_{r}^{2}\left\|\mathbf{g}_{R,k}^{H}\mathbf{\Phi}\right\|^{2}+\sigma_{e,l}^{2}\right)\left(\frac{2}{\tilde{\lambda}_{k,l}}-\frac{\lambda_{k,l}}{\tilde{\lambda}_{k,l}^{2}}\right) \geq \sum_{k=0}^{K}\left|\left(\mathbf{g}_{T,k}^{H}+\mathbf{g}_{R,k}^{H}\mathbf{\Phi}\mathbf{F}\right)\mathbf{w}_{j}\right|^{2}+\sigma_{r}^{2}\left\|\mathbf{g}_{R,k}^{H}\mathbf{\Phi}\right\|^{2}+\sigma_{e,l}^{2}. \tag{15}$$

Then, (13) can be approximated as

$$\sum_{k=0}^{K}2\Re\left\{\tilde{\mathbf{w}}_{k}^{H}\left(\mathbf{g}_{T,l}^{H}+\mathbf{g}_{R,l}^{H}\mathbf{\Phi}\mathbf{F}\right)^{H}\left(\mathbf{g}_{T,l}^{H}+\mathbf{g}_{R,l}^{H}\mathbf{\Phi}\mathbf{F}\right)\mathbf{w}_{k}\right\}-\sum_{k=0}^{K}\left|\left(\mathbf{g}_{T,l}^{H}+\mathbf{g}_{R,l}^{H}\mathbf{\Phi}\mathbf{F}\right)\mathbf{w}_{k}\right|^{2}+\sigma_{r}^{2}\left\|\mathbf{g}_{R,l}^{H}\mathbf{\Phi}\right\|^{2}+\sigma_{e,l}^{2}\geq\Omega_{i}^{\mathrm{in}}. \tag{16}$$

Following the above step, with given Φ, we approximate (8a)–(8d) into the following convex problem with respect to (w.r.t.) $\{\mathbf{w}_k\}_{k=0}^{K}$.

$$\text{P1:}\ \max_{\mathbf{w}_k,r_k,\lambda_{k,l},\tau_k}\ \min\tau_k, \tag{17a}$$

$$\text{s.t.}\ \left\|\left[\sqrt{2^{\tau_k+2}},r_k-\lambda_{k,l}\right]\right\|\leq r_k+\lambda_{k,l},\forall k,\forall l, \tag{17b}$$

$$(14),(15),(16),(8c),(8d). \tag{17c}$$

Then, we will handle the problem w.r.t. Φ with given $\{\mathbf{w}_k\}_{k=0}^{K}$.

Firstly, around the given point $(\tilde{\Phi},\tilde{r}_k,\tilde{\lambda}_{l,k})$, we have

$$\frac{2\Re\left\{\mathbf{w}_{k}^{H}\left(\mathbf{h}_{T,k}^{H}+\mathbf{h}_{R,k}^{H}\widetilde{\mathbf{\Phi}\mathbf{F}}\right)^{H}\left(\mathbf{h}_{T,k}^{H}+\mathbf{h}_{R,k}^{H}\mathbf{\Phi}\mathbf{F}\right)w_{k}\right\}}{\tilde{r}_{k}-1}-\frac{\left|\left(\mathbf{h}_{T,k}^{H}+\mathbf{h}_{R,k}^{H}\widetilde{\mathbf{\Phi}\mathbf{F}}\right)\mathbf{w}_{k}\right|^{2}}{\left(\tilde{r}_{k}-1\right)^{2}}\left(r_{k}-1\right) \geq \sum_{j=0,j\neq k}^{K}\left|\left(\mathbf{h}_{T,k}^{H}+\mathbf{h}_{R,k}^{H}\mathbf{\Phi}\mathbf{F}\right)\mathbf{w}_{j}\right|^{2}+\sigma_{r}^{2}\left\|\mathbf{h}_{R,k}^{H}\mathbf{\Phi}\right\|^{2}+\sigma_{i,k}^{2}. \tag{18}$$

Then, we obtain

$$\frac{\sum_{j=0,j\neq k}^{K}2\Re\left\{\mathbf{w}_{j}^{H}\left(\mathbf{g}_{T,k}^{H}+\mathbf{g}_{R,k}^{H}\widetilde{\mathbf{\Phi}\mathbf{F}}\right)^{H}\left(\mathbf{g}_{T,k}^{H}+\mathbf{g}_{R,k}^{H}\mathbf{\Phi}\mathbf{F}\right)\mathbf{w}_{j}\right\}}{\tilde{\lambda}_{k,l}}-\frac{\sum_{j=0,j\neq k}^{K}\left|\left(\mathbf{g}_{T,k}^{H}+\mathbf{g}_{R,k}^{H}\widetilde{\mathbf{\Phi}\mathbf{F}}\right)\mathbf{w}_{j}\right|^{2}}{\tilde{\lambda}_{k,l}^{2}}\lambda_{k,l}+\frac{2\sigma_{r}^{2}\Re\left\{\mathrm{Tr}\left(\tilde{\mathbf{\Phi}}^{H}\mathbf{g}_{R,k}\mathbf{g}_{R,k}^{H}\mathbf{\Phi}\right)\right\}}{\tilde{\lambda}_{k,l}}-\frac{\sigma_{r}^{2}\left\|\mathbf{g}_{R,k}^{H}\tilde{\mathbf{\Phi}}\right\|^{2}}{\tilde{\lambda}_{k,l}^{2}}\lambda_{k,l}+\sigma_{e,l}^{2}\left(\frac{2}{\tilde{\lambda}_{k,l}}-\frac{\lambda_{k,l}}{\tilde{\lambda}_{k,l}^{2}}\right) \geq \sum_{k=0}^{K}\left|\left(\mathbf{g}_{T,k}^{H}+\mathbf{g}_{R,k}^{H}\mathbf{\Phi}\mathbf{F}\right)\mathbf{w}_{j}\right|^{2}+\sigma_{r}^{2}\left\|\mathbf{g}_{R,k}^{H}\mathbf{\Phi}\right\|^{2}+\sigma_{e,l}^{2}. \tag{19}$$

Lastly, (10) can be recast as

$$\sum_{k=0}^{K} 2\Re\left\{\mathbf{w}_k^H\left(\mathbf{g}_{T,l}^H + \mathbf{g}_{R,l}^H\widetilde{\mathbf{\Phi}\mathbf{F}}\right)^H\left(\mathbf{g}_{T,l}^H + \mathbf{g}_{R,l}^H\mathbf{\Phi}\mathbf{F}\right)\mathbf{w}_k\right\} - \sum_{k=0}^{K}\left|\left(\mathbf{g}_{T,l}^H + \mathbf{g}_{R,l}^H\mathbf{\Phi}\mathbf{F}\right)\mathbf{w}_k\right|^2 + 2\sigma_r^2\Re\left\{\mathrm{Tr}\left(\widetilde{\mathbf{\Phi}}^H\mathbf{g}_{R,l}\mathbf{g}_{R,l}^H\mathbf{\Phi}\right)\right\} - \sigma_r^2\left\|\mathbf{g}_{R,l}^H\mathbf{\Phi}\right\|^2 + \sigma_{e,l}^2 \geq \Omega_i^{\text{in}}. \tag{20}$$

Thus, we reformulated (8a)–(8d) as the following convex problem w.r.t. Φ.

$$\text{P2:} \max_{\mathbf{\Phi}, r_k, \lambda_{k,l}, \tau_k} \min \tau_k, \tag{21a}$$

$$\text{s.t.} \left\|\left[\sqrt{2^{\tau_k+2}}, r_k - \lambda_{k,l}\right]\right\| \leq r_k + \lambda_{k,l}, \forall k, \forall l, \tag{21b}$$

$$(18), (19), (20), (8d), (8e). \tag{21c}$$

By combining the above step, we obtain the entail algorithm, which is summarized as Algorithm 1, where each step can be solved by CVX [26].

It should be pointed out that, during the above procedure, we assume that the phase shift is continuous. In fact, we can extend Algorithm 1 to obtain the discrete phase shift $\theta_m^{(d)}$ conveniently. Specifically, we assume that $\theta_m^{(d)}$ equally spaced takes τ values in the circle $\mathcal{F} \triangleq \{0, 2\pi/\tau, \ldots, 2\pi(\tau-1)/\tau\}$ [27]. Then, we project θ_m into $\mathcal{F}$ and select the one which leads to the minimum distance to θ_m as $\theta_m^{(d)}$, i.e., $\theta_m^{(d)} = 2\pi q^\star/\tau$, where $q^\star = \arg\min|\theta_m - 2\pi q/\tau|_{0\leq q\leq\tau-1}$. Here, during each step of the iteration in Algorithm 1, we project the obtained θ_m to $\mathcal{F}$, and set the obtained $\theta_m^{(d)}$ as a fixed point to update $\{\mathbf{w}_k\}_{k=0}^K$ [13].

Now, we analyze the computational complexity of Algorithm 1. Specifically, to optimize $\{\mathbf{w}_k\}_{k=0}^K$, according to [28], the complexity is $\mathcal{O}(3N^2 + 2N)$. Then, to optimize Φ, the complexity is $\mathcal{O}(M^2 + M)$. Hence, the complexity of Algorithm 1 is given by $\mathcal{O}(T\max\{3N^2 + 2N, M^2 + M\})$, where T denotes the number of iterations.

Then, we analyze the convergence of Algorithm 1. In fact, we have

$$G(\mathbf{w}_k, \mathbf{\Phi}) \geq G^\eta(\mathbf{w}_k, \mathbf{\Phi}), G\left(\mathbf{w}_k^\eta, \mathbf{\Phi}^\eta\right) = G^\eta\left(\mathbf{w}_k^\eta, \mathbf{\Phi}^\eta\right), \forall \mathbf{w}_k, \forall \mathbf{\Phi}, \tag{22}$$

where $G(\mathbf{w}_k^\eta, \Phi^\eta)$ and $G^\eta(\mathbf{w}_k^\eta, \Phi^\eta)$ denote the corresponding objective values of (8a)–(8d) and (11a)–(11e), when $\{\mathbf{w}_k, \Phi\} \longleftarrow \{\mathbf{w}_k^\eta, \Phi^\eta\}$. Therefore, we have

$$G\left(\mathbf{w}_k^{\eta+1}, \mathbf{\Phi}^{\eta+1}\right) \overset{(a)}{\geq} G^\eta\left(\mathbf{w}_k^{\eta+1}, \mathbf{\Phi}^{\eta+1}\right) \overset{(b)}{>} G^\eta\left(\mathbf{w}_k^\eta, \mathbf{\Phi}^\eta\right) = G\left(\mathbf{w}_k^\eta, \mathbf{\Phi}^\eta\right), \tag{23}$$

where (b) holds because both $\{\mathbf{w}_k^{\eta+1}, \Phi^{\eta+1}\}$ and $\{\mathbf{w}_k^\eta, \Phi^\eta\}$ are the feasible points and optimal solutions of (8a)–(8d), respectively. Thus, $\{\mathbf{w}_k^{\eta+1}, \Phi^{\eta+1}\}$ is better to (8a)–(8d) than $\{\mathbf{w}_k^\eta, \Phi^\eta\}$. Furthermore, due to (8c)–(8e), the sequence $\{\mathbf{w}_k^\eta, \Phi^\eta\}$ is bounded. Then, according to [29], there exists a sequence $\{\mathbf{w}_k^\eta, \Phi^\eta\}$ with a limit point $\{\mathbf{w}_k^\star, \Phi^\star\}$, i.e.,

$$\lim_{\gamma \longrightarrow +\infty}\left[G\left(\mathbf{w}_k^\eta, \mathbf{\Phi}^\eta\right) - G\left(\mathbf{w}_k^\star, \mathbf{\Phi}^\star\right)\right] = 0, \tag{24}$$

thus completes the proof.

4. Simulation Results

The deployment is given in Figure 2, where there exist one Tx, one RIS, 2 IRs, and 2 ERs. The coordinates of Tx and RIS are (0 m, 0 m, 10 m) and (50 m, 10 m, 10 m), while the IRs and ERs are randomly located in a circle with radius 5 m and centered at (60 m, 0 m, 1.5 m), respectively. The following settings are adopted: $N = 4$, $M = 40$, $\tau = 4$, [6], $\alpha_{n,\max} = 10, \forall n$, [17]. Besides, $\sigma_{i,k}^2 = \sigma_{e,l}^2 = -80$ dBm, $\forall k, \forall l$, and $\sigma_r^2 = -80$ dBm [19], and $a_l = 1500$, $b_l = 0.0022$, and $R_l = 3.9$ mW [24]. The other parameters are the same as those in [13].

We compare the proposed scheme with the following baselines: (1) the discrete phase shift scheme; (2) the passive RIS with relay scheme [12]; (3) the passive RIS-assisted scheme; (4) the no RIS case, which are labeled as "Active RIS," "Discrete," "Relay" "Passive RIS," "No RIS," respectively.

Figure 3 shows the obtained secrecy rate versus the number of iterations with different N and M. From Figure 3, we can see that the secrecy rate always increases with the iteration numbers and converges within 20 iterations, which verifies the convergence of the AO method.

First, we show the secrecy rate versus P_s in Figure 4. As we can see, the secrecy rate increases with P_s, and all RIS-aided schemes outperform the no-RIS-aided designs. Besides, the active RIS scheme significantly outperforms the passive RIS design, since the power amplification can alleviate the impact of "double fading." Thus, the received signal power at the IRs is enhanced. The discrete phase shifts suffer certain performance losses when compared with the continuous case. However, the loss is very slight, which suggested the effectiveness of the discrete operation. In addition, we can see that the proposed design outperforms the passive RIS with a relay scheme, mainly due to the reason that the passive RIS with a relay scheme needs two continuous time slots to achieve information transmission [30].

Then, we show the secrecy rate versus M in Figure 5, where we can see that for all these methods, the secrecy rate tends to increase with M. This is because more signals can reach the RIS with larger M. Besides, active RIS obtains better performance than passive RIS.

Next, we show the secrecy rate versus the EH constraint in Figure 6, where we can see that the secrecy rate decreases with the EH threshold. Since with a higher threshold, more signals need to transmit in the ER's channel, and thus, the secrecy rate tends to decrease.

Lastly, Figure 7 plots the secrecy rate versus the Tx-RIS distances, where the RIS moves along the x-axis from the Tx to the IR's area. From this figure, we can see that the active RIS scheme outperforms the passive RIS scheme in the considered region. Moreover, for active RIS, the secrecy rate increases when RIS moves from the Tx to the IR's area, while for passive RIS, the secrecy rate first decreases to a low point and then increases. Besides, whether for active RIS or passive RIS, when

(1) Initialize a feasible point $(\{\mathbf{w}_k^0\}_{k=0}^K, \Phi^0)$, choose $\eta = 0$;
(2) **repeat**
  (a) Obtain $\{\mathbf{w}_k^\eta\}_{k=0}^K$ by solving (17);
  (b) Obtain Φ^η by solving (21);
  (c) Update $(\{\tilde{\mathbf{w}}_k\}_{k=0}^K, \tilde{\Phi}) \leftarrow (\{\mathbf{w}_k^\eta\}_{k=0}^K, \Phi^\eta)$;
  (d) $\eta \leftarrow \eta + 1$;
(3) **until** Converge.
(4) **Output** $(\{\mathbf{w}_k^\star\}_{k=0}^K, \Phi^\star)$.

Algorithm 1: The AO algorithm

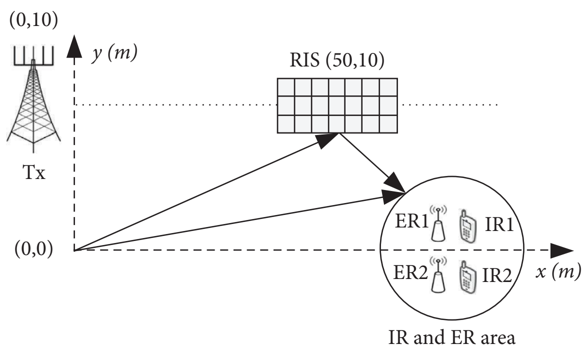

Figure 2: Simulation deployment.

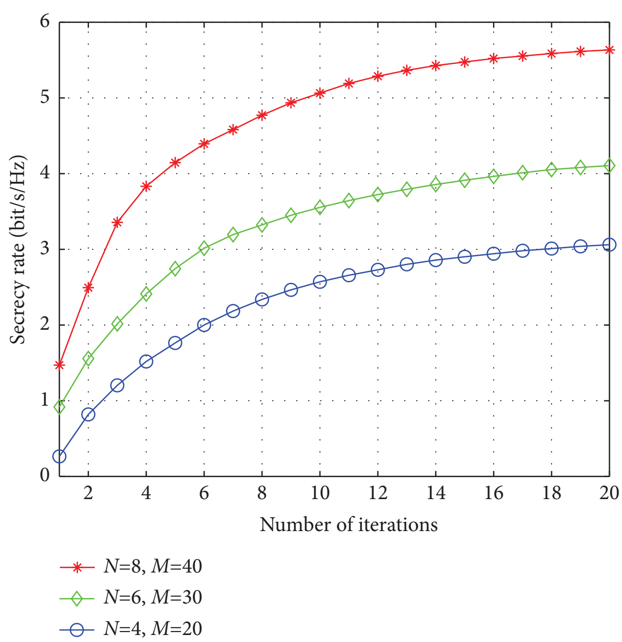

Figure 3: Convergence.

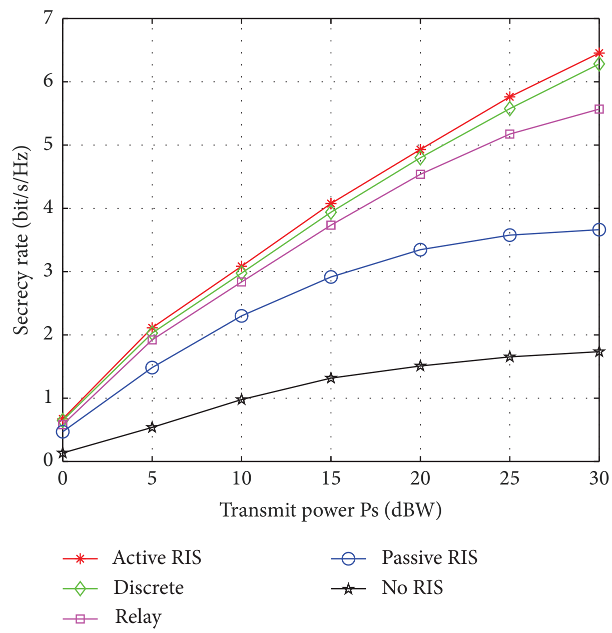

Figure 4: Secrecy rate versus the transmit power.

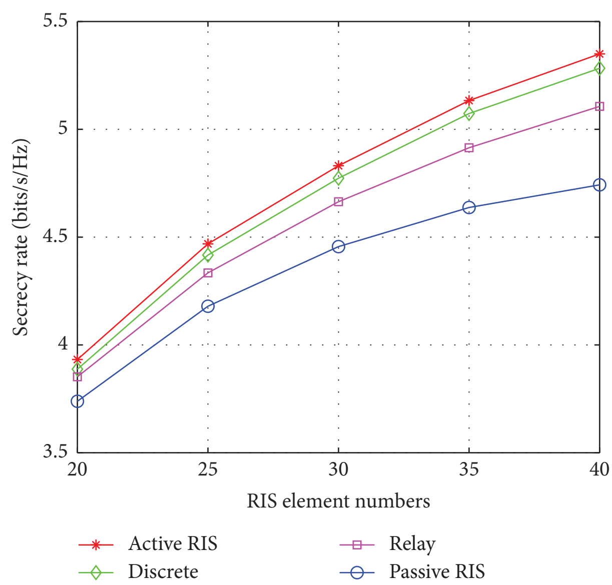

Figure 5: Secrecy rate versus the number of RIS elements.

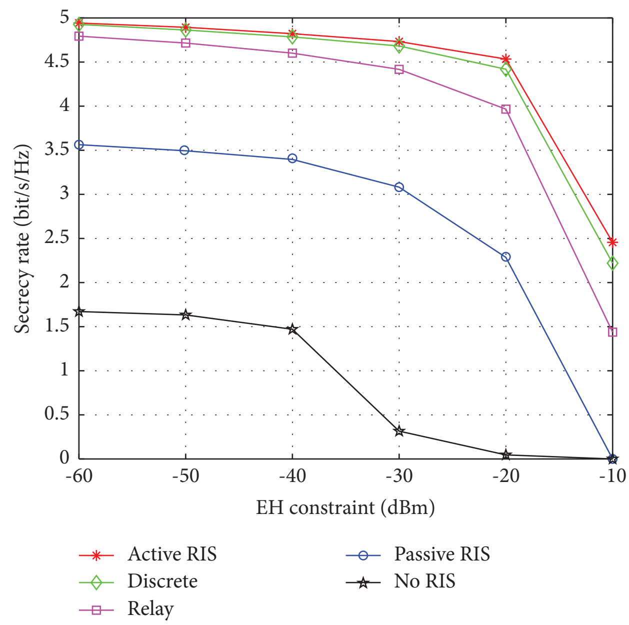

FIGURE 6: Secrecy rate versus the EH constraint.

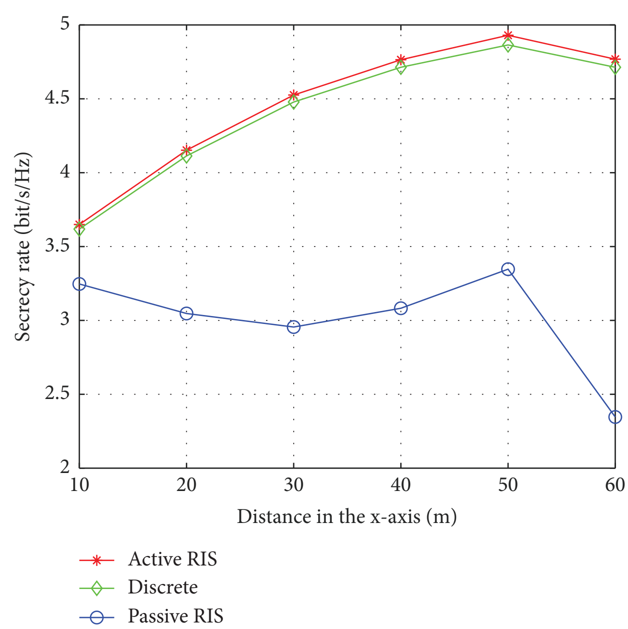

FIGURE 7: Secrecy rate versus the RIS location.

RIS moves away from the user area, the secrecy rate decreases. Thus, it is better to deploy the active RIS near the IRs.

5. Conclusion

We investigated the active RIS-assisted secure SWIPT networks, where an AO algorithm was proposed to design the BF and RC to handle the fairness secrecy rate objective subject to the nonlinear EH constraints and the transmit power constraints. The simulation result verified the performance of the proposed scheme.

Appendix

Following equation (8b), we can see that to satisfy

$$E_l^{\text{prac}} = \frac{R_l/1 + e^{-a_l\left(E_l^{\text{in}} - b_l\right)} - R_l/1 + e^{a_l b_l}}{1 - 1/1 + e^{a_l b_l}} \geq E_{\text{th}}, \tag{A.1}$$

one must have

$$\begin{aligned}
&\frac{R_l}{1+e^{-a_l\left(E_l^{\text{in}}-b_l\right)}} \geq E_{th}\left(1-\frac{1}{1+e^{a_l b_l}}\right)+\frac{R_l}{1+e^{a_l b_l}}\\
&\Rightarrow e^{-a_l\left(E_l^{\text{in}}-b_l\right)} \leq \frac{R_l}{E_{th}\left(1-\left(1/1+e^{a_l b_l}\right)\right)+\left(R_l/1+e^{a_l b_l}\right)}-1\\
&\Rightarrow a_l b_l - a_l E_l^{\text{in}} \leq \ln\left(\frac{R_l}{E_{th}\left(1-\left(1/1+e^{a_l b_l}\right)\right)+\left(R_l/1+e^{a_l b_l}\right)}-1\right)\\
&\Rightarrow E_l^{\text{in}} \geq b_l - \frac{\ln\left(R_l/E_{th}\left(1-\left(1/1+e^{a_l b_l}\right)\right)+\left(R_l/1+e^{a_l b_l}\right)-1\right)}{a_l}\\
&\Rightarrow \sum_{k=0}^{K}\left|\left(\mathbf{g}_{T,l}^H+\mathbf{g}_{R,l}^H\mathbf{\Phi}\mathbf{F}\right)\mathbf{w}_k\right|^2+\sigma_r^2\left\|\mathbf{g}_{R,l}^H\mathbf{\Phi}\right\|^2 \geq \Omega_l^{\text{in}}.
\end{aligned} \tag{A.2}$$

Thus, we finish the derivation.

Data Availability

Data are available upon request.

Conflicts of Interest

The authors declare that there are no conflicts of interest regarding the publication of this article.

Acknowledgments

This work was supported by the Industry-University-Research Cooperation Project of Jiangsu Province under Grant no. BY2018282.

References

[1] Q. Wu, G. Y. Li, W. Chen, D. W. K. Ng, and R. Schober, "An overview of sustainable green 5G networks," *IEEE Wireless Communications*, vol. 24, no. 4, pp. 72–80, 2017.

[2] G. Huang and W. Tu, "Joint power splitting and power allocation for two-way OFDM relay networks with SWIPT," *Computer Communications*, vol. 124, pp. 76–86, 2018.

[3] X. Huang, J. He, Q. Li, Q. Zhang, and J. Qin, "Optimal power allocation for multicarrier secure communications in full-duplex decode-and-forward relay networks," *IEEE Communications Letters*, vol. 18, no. 12, pp. 2169–2172, 2014.

[4] Q. Li, Q. Zhang, and J. Qin, "Beamforming for information and energy cooperation in cognitive non-regenerative two-way relay networks," *IEEE Transactions on Wireless Communications*, vol. 15, no. 8, pp. 5302–5313, 2016.

[5] Y. Wu, A. Khisti, C. Xiao, G. Caire, K.-K. Wong, and X. Gao, "A survey of physical layer security techniques for 5G wireless networks and challenges ahead," *IEEE Journal on Selected Areas in Communications*, vol. 36, no. 4, pp. 679–695, 2018.

[6] Q. Wu, S. Zhang, B. Zheng, C. You, and R. Zhang, "Intelligent reflecting surface aided wireless communications: a tutorial," *IEEE Transactions on Communications*, vol. 69, no. 5, pp. 3313–3351, 2021.

[7] Y. Liu, X. Liu, X. Mu et al., "Reconfigurable intelligent surfaces: principles and opportunities," *IEEE Communications Surveys and Tutorials*, vol. 23, no. 3, pp. 1546–1577, 2021.

[8] Z. Li, W. Chen, Q. Wu, K. Wang, and J. Li, "Joint beamforming design and power splitting optimization in IRS-assisted SWIPT NOMA networks," *IEEE Transactions on Wireless Communications*, vol. 21, no. 3, pp. 2019–2033, 2022.

[9] H. Niu, Z. Chu, F. Zhou, Z. Zhu, L. Zhen, and K.-K. Wong, "Robust design for intelligent reflecting surface assisted secrecy SWIPT network," *IEEE Transactions on Wireless Communications*, vol. 21, no. 6, pp. 4133–4149, 2022.

[10] Z. Lin, H. Niu, K. An et al., "Refracting RIS aided hybrid satellite-terrestrial relay networks: joint beamforming design and optimization," *IEEE Transactions on Aerospace and Electronic Systems*, vol. 58, no. 4, pp. 3717–3724, 2022.

[11] H. Xie, J. Xu, and Y. F. Liu, "Max-min fairness in IRS-aided multi-cell MISO systems with joint transmit and reflective beamforming," *IEEE Transactions on Wireless Communications*, vol. 20, no. 2, pp. 1379–1393, 2021.

[12] Z. Luo and G. Huang, "Energy-efficient mobile edge computing in RIS-aided OFDM-NOMA relay networks," *IEEE Transactions on Vehicular Technology*, pp. 1–16, 2022.

[13] H. Niu, Z. Chu, F. Zhou, Z. Zhu, M. Zhang, and K.-K. Wong, "Weighted sum secrecy rate maximization using intelligent reflecting surface," *IEEE Transactions on Communications*, vol. 69, no. 9, pp. 6170–6184, 2021.

[14] Y. Sun, K. An, Y. Zhu et al., "Energy-efficient hybrid beamforming for multi-layer RIS-assisted secure integrated terrestrial-aerial networks," *IEEE Transactions on Communications*, vol. 70, no. 6, pp. 4189–4210, 2022.

[15] Q. Wang, F. Zhou, R. Q. Hu, and Y. Qian, "Energy efficient robust beamforming and cooperative jamming design for IRS-assisted MISO networks," *IEEE Transactions on Wireless Communications*, vol. 20, no. 4, pp. 2592–2607, 2021.

[16] Y. Sun, K. An, J. Luo, Y. Zhu, G. Zheng, and S. Chatzinotas, "Intelligent reflecting surface enhanced secure transmission against both jamming and eavesdropping attacks," *IEEE Transactions on Vehicular Technology*, vol. 70, no. 10, pp. 11017–11022, 2021.

[17] R. Long, Y.-C. Liang, Y. Pei, and E. G. Larsson, "Active reconfigurable intelligent surface-aided wireless communications," *IEEE Transactions on Wireless Communications*, vol. 20, no. 8, pp. 4962–4975, 2021.

[18] C. You and R. Zhang, "Wireless communication aided by intelligent reflecting surface: active or passive?" *IEEE Wireless Communications Letters*, vol. 10, no. 12, pp. 2659–2663, 2021.

[19] K. Liu, Z. Zhang, L. Dai, S. Xu, and F. Yang, "Active reconfigurable intelligent surface: fully-connected or sub-connected?" *IEEE Communications Letters*, vol. 26, no. 1, pp. 167–171, 2022.

[20] K. Zhi, C. Pan, H. Ren, K. K. Chai, and M. Elkashlan, "Active RIS versus passive RIS: which is superior with the same power budget?" *IEEE Communications Letters*, vol. 26, no. 5, pp. 1150–1154, 2022.

[21] L. Dong, H.-M. Wang, and J. Bai, "Active reconfigurable intelligent surface aided secure transmission," *IEEE Transactions on Vehicular Technology*, vol. 71, no. 2, pp. 2181–2186, 2022.

[22] P. Niu, J. Zhu, L. Wei et al., "Application of fluorescent probes in reactive oxygen species disease model," *Critical Reviews in Analytical Chemistry*, pp. 1–36, 2022.

[23] Y. Wang, Z. Lin, H. Niu et al., "Secure satellite transmission with active reconfigurable intelligent surface," *IEEE Communications Letters*, vol. 26, no. 12, pp. 3029–3033, 2022.

[24] Z. Zhu, N. Wang, W. Hao, Z. Wang, and I. Lee, "Robust beamforming designs in secure MIMO SWIPT IoT networks with a non-linear channel model," *IEEE Internet of Things Journal*, vol. 8, no. 3, pp. 1702–1715, 2021.

[25] A. S. Vishwanathan, A. J. Smola, and S. V. N. Vishwanathan, "Kernel methods for missing variablesl," *Proc. Int. Workshop Artif. Intell. Stat.*vol. 25, pp. 325–332, 2005.

[26] M. Grant and S. Boyd, "CVX: Matlab Software for Disciplined Convex Programming," 2013, http://cvxr.com/cvx/.

[27] D. Li, "Ergodic capacity of intelligent reflecting surface-assisted communication systems with phase errors," *IEEE Communications Letters*, vol. 24, no. 8, pp. 1646–1650, 2020.

[28] K. Y. Wang, A. M. C. So, T.-H. Chang, W. K. Ma, and C.-Y. Chi, "Outage constrained robust transmit optimization for multiuser MISO downlinks: tractable approximations by conic optimization," *IEEE Transactions on Signal Processing*, vol. 62, no. 21, pp. 5690–5705, 2014.

[29] A. A. Nasir, H. D. Tuan, T. Q. Duong, and H. V. Poor, "Secrecy rate beamforming for multicell networks with information and energy harvesting," *IEEE Transactions on Signal Processing*, vol. 65, no. 3, pp. 677–689, Feb. 2017.

[30] M. Obeed and A. Chaaban, "Joint beamforming design for multiuser MISO downlink aided by a reconfigurable intelligent surface and a relay," *IEEE Transactions on Wireless Communications*, vol. 21, no. 10, pp. 8216–8229, 2022.